1. Selecting electrons in ATIC

ATIC is a calorimetric instrument and, as such, relies upon the difference in the development of the cascades (showers) initiated by protons and electrons. Moreover, the atmospheric gamma rays provide a calibration for the electron analysis and suffer from very little proton contamination. The method employed here is described in detail in ref. 12, is nearly identical to that used in the BETS analysis[32] and in emulsion chamber work[8,9] and has been extensively studied by Monte-Carlo (GEANT and FLUKA) simulation.[s1,s2,s3]

In a calorimeter instrument such as ATIC with a distributed interaction target above the active BGO calorimeter, a proton must interact to produce pions which then decay (or interact) to initiate the hadronic cascade. The leading proton can itself interact again (usually in the BGO) to produce additional pions and a second generation shower. In order to mimic an electron, the proton must interact early in the target and produce only a few pions. However, the 30 cm thick target region provides ample space for the interaction products to spread laterally before reaching the BGO calorimeter. Moreover, as the energy increases the mean multiplicity emerging from a proton interaction increases. Together these lead to a laterally wider shower profile when compared to electrons and gamma rays.

An electron (or gamma ray) produces a photon (or e^+-e^- pair) in the 1.5 radiation lengths of material above the BGO. These secondaries then produce additional photons and pairs in a rapidly increasing electromagnetic (EM) cascade whose properties have been known for many decades and for which detailed calculation codes have been developed. Since there is no Fermi momentum involved and multiple scattering is unimportant at these high energies, the cascades do not spread, laterally, as do the hadronic cascades. Moreover, the EM cascade rapidly absorbs

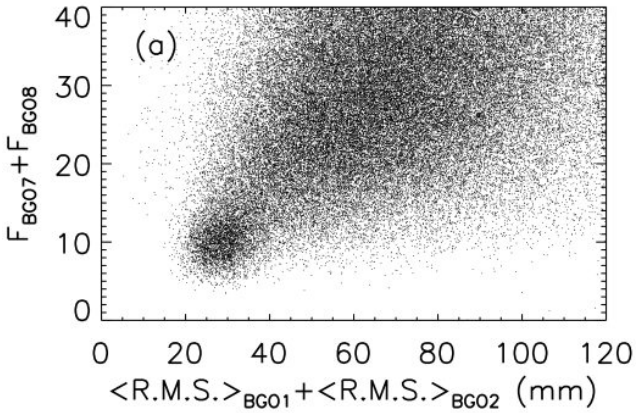

Figure s1a. Scatter plot (for> 50 GeV events) after trajectory selection (see caption to Figure 1 in paper for parameter definitions).

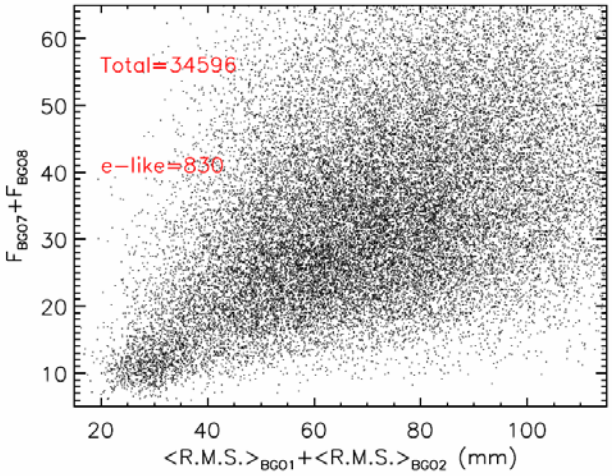

Figure s1b. Scatter plot similar to Figure s1a, but for >100 GeV events.

the incident particle energy, the majority of which is actually deposited in the fully active BGO calorimeter (~85% vertical incidence at 150 GeV), including the shower maximum. In contrast, hadronic cascades deposit only ~35% of their energy in the BGO crystals. At the bottom of the calorimeter, electron showers have little energy remaining while hadronic cascades have a large residual energy in the shower.

Here we show the general electron analysis procedure, step by step. First we build the trajectory, and find the 'charge' of the incident particle in the top silicon matrix. Most electrons will pass this cut, but about 26% of the total events will be rejected. Figure s1a and s1b shows the scatter plot between the F parameter in the bottom two BGO layers versus the shower width (R.M.S.) in the top two layers of the calorimeter after the trajectory analysis (c.f. Figure 1 in the main text).

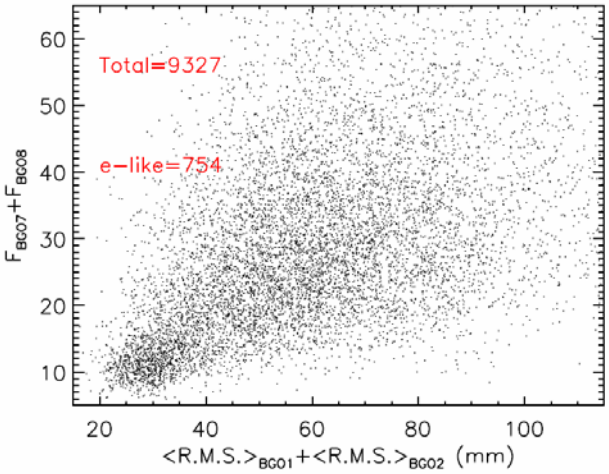

Figure s2. Scatter plot (for > 100 GeV events) after shower profile fitting..

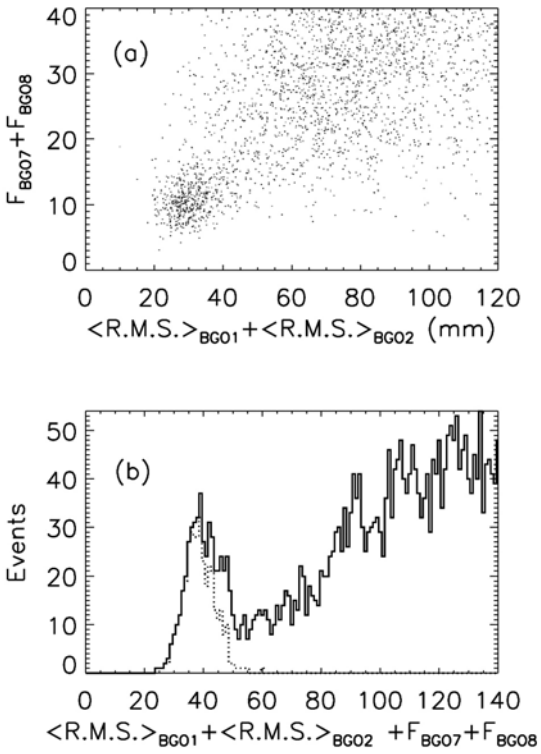

Figure s3. Scatter plot for gamma-ray candidates (a) and simple histogram of the measured parameters (b). The dashed histogram shows the gamma-ray events..

Next, for each event we fit the energy deposited in each layer to an EM cascade profile at an energy corresponding to the total event energy seen in the calorimeter. This is used to estimate the cascade starting point. The starting point of most electron showers are above the first BGO layer, but a large fraction of the proton cascades have not started and, consequently, will be rejected during this step. Figure s2 shows a scatter plot, similar to Figure s1b, after the profile selection. (Note that only 9% of the electrons are removed while 73% of the proton background is eliminated.)

A similar analysis is applied to the gamma-ray candidate events to determine the next cut. The gamma-ray candidates are identified using two modules (Si-matrix and Scintillator strips), on the top of ATIC, that measure the charge of incident particles. For gamma-ray detection in ATIC, the charge modules are used as an

anticoincidence system in the off-line data analysis. Since backscattering from the shower in the calorimeter is almost isotropic, we can choose several strips or pixels around the incident trajectory to act as this anticoincidence. The proton background among gamma-ray candidates is heavily suppressed since for a real proton to leave a small to zero signal in the Silicon Matrix, i.e. to be classified as a gamma-ray candidate, the proton must just clip the edge of one of the pixels and go through the next gap between pixels. The acceptance for such trajectories is very small. Figure s3a shows an equivalent scatter plot for ~1600 gamma-ray candidates, while Figure s3b shows a histogram made simply from the data in (a). The gamma-ray separation is easily seen.

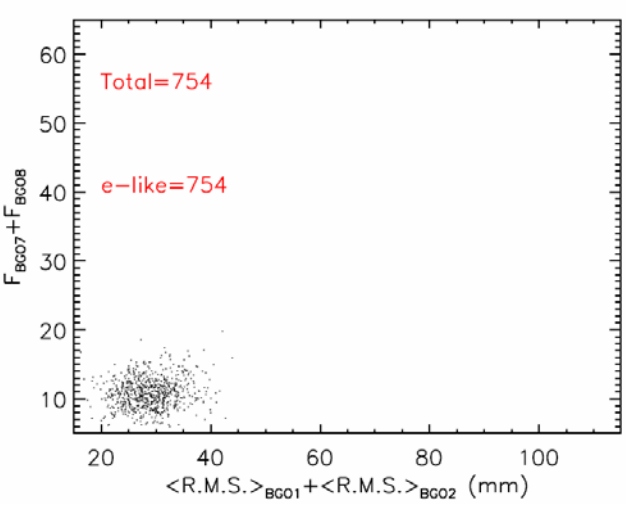

Figure s4. Scatter plot (for >100 GeV events) after electron selection using <R.M.S.> and F value cuts.

The final step in separating electrons from the proton background is to make a cut on both the appropriate F value and <R.M.S.> histograms.[10] Since the location of this cut is weakly dependent on energy, we utilize the gamma-ray data at the same deposited energy to guide the cut selection. This is then compared to FLUKA Monte-Carlo simulations which predict the optimum location for the cuts. The final result is the scatter plot shown in Figure s4.

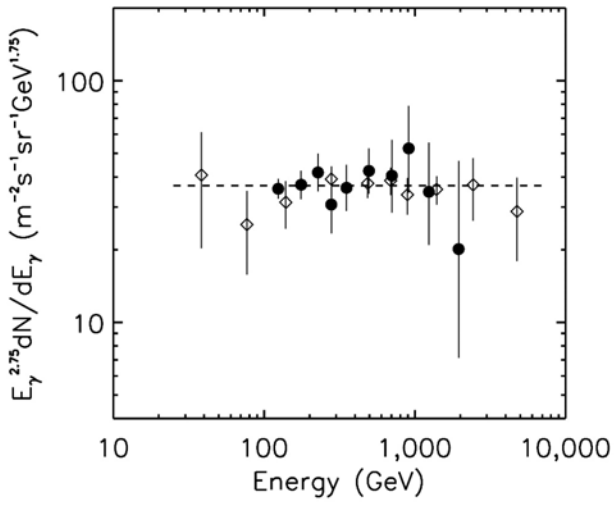

Figure s5. Gamma-rays, produced by proton interactions in the residual atmosphere above the balloon, follow the incident proton energy spectrum ($E^{-2.75}$) and provide a calibration for the electron-proton separation and a validation of the overall technique. Errors are one sigma.

We can also use the gamma-ray events to calibrate any energy dependence in the efficiency of the selection process. Since these are atmospheric secondary gamma rays, their energy spectrum should follow that of the parent proton spectrum. Such results are shown in Figure s5 which compares ATIC results to previous work from emulsion chamber analyses[9] and from calculations of the anticipated spectrum. ATIC records these events with a reduced efficiency (due to triggering constraints), but the gamma rays provide a means to cross-check the electron analysis since electron and gamma-ray cascades are identical in the BGO calorimeter.[12,13] A total of 313 gamma rays above 100 GeV

have been analyzed and are shown in the figure, scaled by $E^{+2.75}$ and normalized to 4 g/cm^2 atmospheric overburden for ATIC-1+2 (solid circles) compared to calculations[8] (dashed line) and to emulsion chamber data (open diamonds).[8,9] The agreement between different experimental results and with the calculated distribution is a validation of the ATIC analysis technique.

Finally, we correct the incident energy for each selected electron (or gamma-ray) event for the energy that leaves the bottom of the calorimeter. Using the ratio of the energy deposited in the last BGO layer to the total energy deposited in the calorimeter, a correction is applied to better align the event energies as illustrated in Figure s6 for a set of Monte-Carlo generated events at 150 GeV. The energy resolution exhibited by the dotted histogram is ≈ 2%. The tail on the distribution is due to the uncertainty in the cascade starting points.

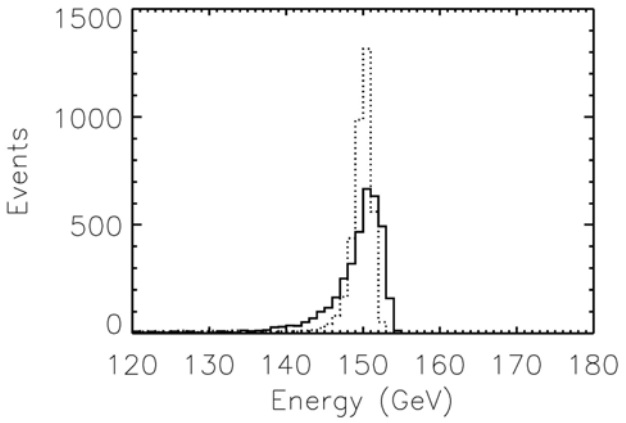

Figure s6. Histograms of simulated electron events at 150 GeV. The energies assigned by using only the BGO signal are represented by the solid curve. The results, after correction for lost energy, are shown as the dotted histogram which is narrower, with much less of a tail.

2. Validating the Selection Results

Figure s7 shows the charge distribution observed in the Silicon matrix detector at the top of the ATIC experiment for all events with energy deposit above 50 GeV. Several features are clearly discernible, e.g. the He (alpha particle) peak and peaks at charge 6 and 8 corresponding to primary C and O nuclei, respectively. An analysis has been performed assuming that all of these events are electron candidates,[s3] following the procedures just described except not using the measured charge of the particle. The dashed line, after electron selection, shows that almost all of the heavy primaries (charge above 3.5) have been rejected, and even the He peak cannot be found with statistical significance. Only 12 heavy primaries from the sample of 126,157 $Z \geq 3.5$ events have passed the electron selection, which implies a rejection factor of 1 in 8000 to 1

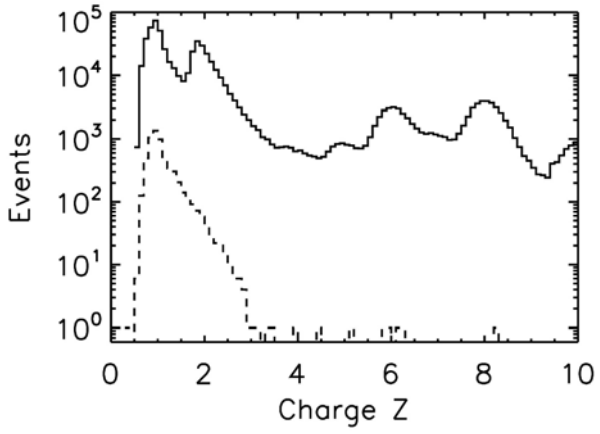

Figure s7. Charge distribution from the Silicon matrix detector. Solid: all particles; dashed: The charge distribution after electron selection.

in 15,000, consistent with the calibration data from the CERN SPS runs. (There are two more charge detectors with somewhat lower charge resolution, scintillators 1 and 2; the results from them -- not shown here -- look very similar to that of the silicon matrix.)

This result is for all events with energy deposited in the calorimeter >50 GeV. If we restrict the data to events with >200 GeV energy deposit, 2 events survive out of 22,748, with a rejection of ~ 1 in 11,000. For a cut at >500 GeV, zero heavy primaries survive out of 5345 events, as expected. In detail, such an analysis shows that the rejection power is approximately constant over the energy range investigated.

The ATIC data are analyzed in terms of the energy deposited in the calorimeter. For electrons this is ≥ 85% of the actual energy of the incident particle. For hadronic showers, however, the energy deposit is only ~35% of the incident energy. Thus, at a given energy deposit, the hadron energy that can lead to confusion with a real electron must come from a higher incident energy (where there are fewer hadronic particles). Using the known spectral indices for electrons and hadrons, this energy difference increases the hadronic rejection by a factor of ~5. However, Z ≥ 2 particles are not the same as protons, since they contain more nucleons giving a high probability of multi-nucleon interactions which can broaden the ensuing shower thus making them easier to reject than would be an equivalent proton. The difference between Z ≥ 2 and proton showers has been studied with detailed FLUKA Monte Carlo simulations which show that Z ≥ 2 particles are easier to reject by a factor of ~8 compared to protons. Thus, the equivalent proton rejection factor becomes 5/8 of 1 in 10,000 or about 1 in 6000. This is the result used to determine the unresolved proton background component of the combined background that is shown as the open triangles in Figure 2 in the printed version.

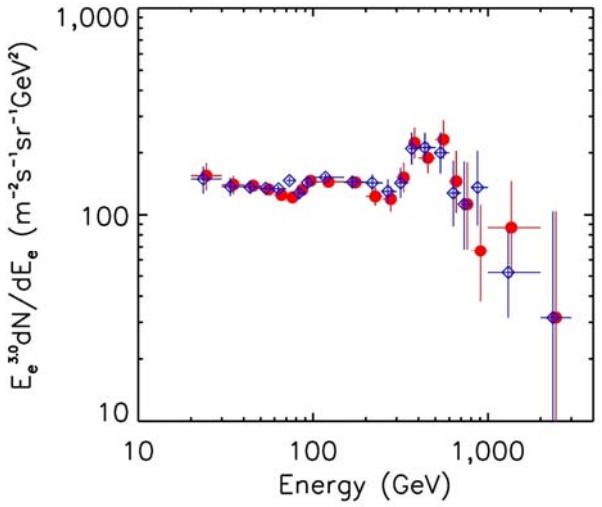

Figure s8. The energy spectra (multiplied by E^3) resulting from the two different methods of determining the energy of the electron selected events. Solid red dots show the result from using the total deposited energy in the calorimeter while the open blue diamonds show the spectra obtained using the shower maximum in the longitudinal shower development profile to determine the incident energy.[s4] One sigma uncertainty limits are shown.

There is a second cross-check that was performed. In experiments such as BETS and Emulsion chambers, the energy of the incident particle is determined according to the shower profile and the location of the shower maximum. If the incident particle is an electron or gamma-ray, the shower maximum or shower profile can determine the particle energy, but if the incident particle is a proton, the shower max/profile method will give erroneous results.

Figure s8 shows electron spectra which are obtained from the two different methods for the ATIC-2 data. For the electron/gamma events selected as described above, the two methods are in substantial agreement, which implies that these are indeed EM cascades. The slight difference between the two results is due to the different energy resolution of the two methods. The energy resolution of the shower profile method is about 15%,[s4] but for ATIC, the energy resolution is ~2% as measured at the CERN SPS with 150 GeV electrons[s5] and shown in Figure s6.

3. Comparison with other electron measurements

The highest resolution measurements prior to ATIC came from balloon-borne,[31] and space exposed[30] magnetic spectrometer experiments. These traced out the electron spectrum below 100 GeV and provided the normalization for interstellar propagation calculations. A calorimetric experiment[32], using techniques similar to those described here, but having a thinner calorimeter, has also made measurements below 100 GeV which are in good agreement with the magnetic spectrometer results. ATIC also agrees with this accumulated dataset at low energy.

At higher energies, the only results available, prior to ATIC were the data from a long series of Emulsion Chamber (EC) flights. A typical EC is composed of layers of electron sensitive nuclear photographic emulsion interleaved with thin lead plates and with high sensitivity x-ray films. The cascades induced by high energy particles are recorded in the emulsion and leave dark spots on the developed x-ray films. Scanning of the films is done manually to identify high energy cascades which are then followed, upward, to the cascade starting point. Tracing the incident particle to the top of the stack allows identification of Z=1 primaries and the shower first interaction point. After checking the secondary tracks around the first interaction point by visual inspection, electron events are selected from the large amount of proton background. Typical EC configurations have ~7 radiation lengths of material in the calorimeter portion and electron-proton separation is achieved through fitting the cascade intensity, as a function of depth into the calorimeter, to an electromagnetic shower profile. Estimating the depth of the shower maximum provides a measure of the incident particle energy with an energy resolution of ~15%.[s4].

Accumulating this dataset was a remarkable achievement, requiring much laborious scanning and measuring to obtain the events. Not all events in a specific EC flight could be analyzed, and attention was devoted, usually, to the highest energy events. The results from many flights had to be put together, estimating the energy dependent exposure for each to obtain the

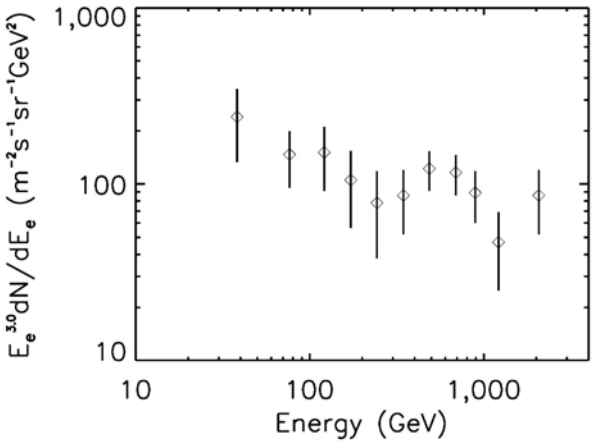

Figure s9. Emulsion chamber electron spectrum at the top of the atmosphere.[9] One sigma errors.

final dataset. Unfortunately, due to the labor intensive analysis procedure, only a limited sample could be analyzed.

As shown in Figure s9, the EC data decrease sharply with energy. While of limited statistical significance, the EC results do show an enhancement in the 500-900 GeV energy range, relative to the declining spectrum observed at the lower energies. These points also show the smallest uncertainty. Qualitatively, this enhancement is consistent with the excess reported here by ATIC. Thus, the present results are not in conflict with the EC data.

4. Significance of the Electron Excess

The ATIC result is based upon the observation of 210 electrons between 300 and 800 GeV compared to the anticipated number from the "general", secondary component (as calculated by GALPROP) of 140 events. Statistically, this gives a significance of 5.9, i.e. ~6 as stated in the text. However, in the past, there had been questions raised about using this simple formalism, particularly for discussing the significance of a detection of a new source in gamma-ray astronomy. A more conservative method was developed[15] to estimate significance which takes the form

$$S = \frac{N_s}{\hat{\sigma}(N_s)} = \frac{N_{on} - \alpha N_{off}}{\sqrt{\alpha(N_{on} + N_{off})}}, \text{with } \alpha = 1.$$

Using N_{on} = 210 and N_{off} = 140 results in a significance value of 3.75, i.e. ~4 as stated in the text. This is above the value usually assumed for a source detection of 2.5-3.0.

The result presented here is relative to the expected background as given by the GALPROP curve. This curve involves the best physics of galactic propagation that is available. None-the-less, it is possible to vary some of the parameters and still remain consistent with the measured data. This leads to a range of spectral indices that each predict a different background level. For the range of values that are consistent with the data, the significance level can vary by ±0.7.

5. Astrophysical Source Models

The excess in the electron spectrum may be explainable as the contribution of a nearby source, provided such a source can be found with the needed spectrum and intensity. The sharp decrease in the excess electrons observed by ATIC between 600-800 GeV requires a source with such a cut-off. Young supernova remnants (SNR) such as Vela, show accelerated particles to 10's of TeV or higher, as evidenced by the observations of the "TeV" gamma ray spectrum. Middle-aged SNR have a lower maximum energy for particle acceleration, due to the weakening of the shock wave with expansion time, and may be more likely candidates to explain the ATIC results. Kobayashi et al.[4] have modeled several such sources as shown in Figure s10. The

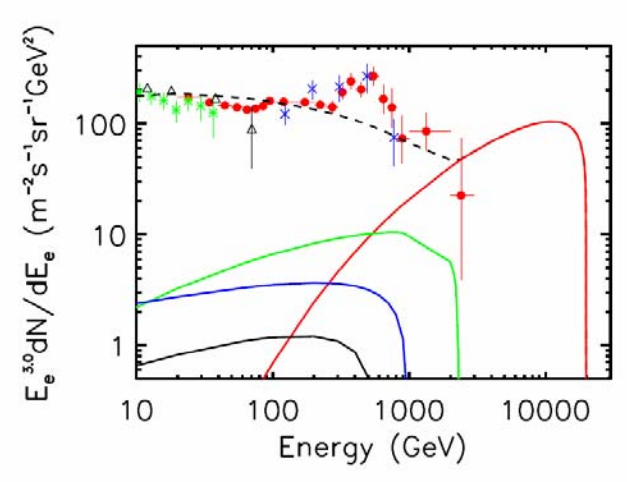

Figure s10. The possible contribution to the electron spectrum from nearby sources; Vela (red), Monogem (green), Loop 1 (blue) and Geminga (black).

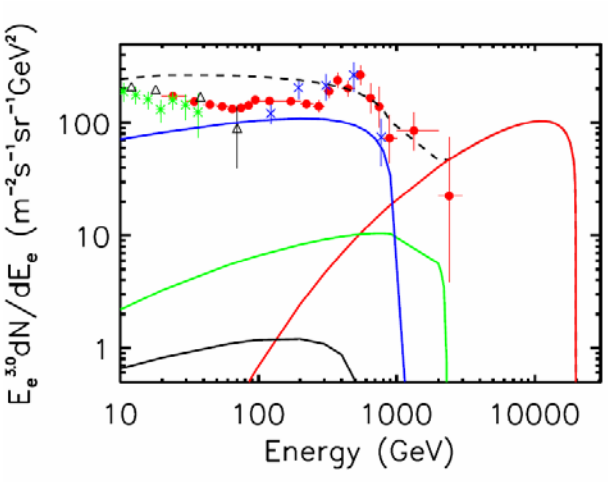

Figure s11. Predicted electron spectrum for a Loop 1 source with its intensity scaled by a factor of 30.

high energy cut-off of sources such as Loop 1 and Geminga makes them candidates. Kobayashi et al.[4] modeled the source production and propagation to the Earth for a large selection of source and propagation parameters, and the set of parameters giving the lowest cut-off energies were selected for Fig. s10.

To compare these sources to the ATIC data shown at the top of the figure, the source intensity is scaled so as to pass through the ATIC data near 500 GeV. The result for Loop 1 (scaled by a factor of 30) is shown in Figure s11 while the result for Geminga (scaled by a factor of 60) is shown in Figure s12. In both cases the electrons from the source have been added to the general electron spectrum calculated by GALPROP. The predicted spectra are shown as the dashed lines.

The difficulty here is that the source spectrum, plus the effects of propagation extend the contribution to low energies, giving a result that is in disagreement with the well measured data below 100 GeV. This is a fundamental limitation of such source models. While small changes may be made by optimizing model parameters, the SNR acceleration model cannot reproduce both the low energy and high energy data. Moreover, it is difficult to understand how such sources can output 30-60 times more energy in accelerated electrons than the model predicts.

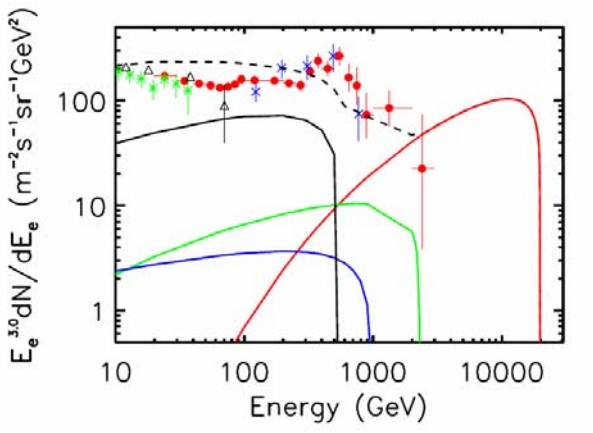

Figure s12. Predicted electron spectrum for a Geminga source with its intensity 60 times higher than the model.

6. Dark Matter Source Models

The nature of dark matter remains one of the most intriguing questions in modern physics. Many suggestions have been made for the identity of these "Weakly Interacting Massive Particles" (WIMPS), and there are active underground experimental programs designed to detect different types of WIMPs. Moreover, if the dark matter particle is a manifestation of certain types of "physics beyond the standard model", supersymmentry, then the coming experiments at the CERN LHC may discover such particles.

There is, also, increasing interest in indirect searches for dark matter due to the development of new balloon and space experiments. Indirect searches attempt to measure the gamma-rays, proton-anti-proton pairs and e^+-e^- pairs that result directly as products of dark matter annihilation or as secondaries of such products. In all cases, the dark matter "signal" must be detected above the natural background produced by cosmic rays from primary acceleration sites propagating through the galaxy. Neutralinos, from supersymmetic modes produce gamma-rays, and these would be observed as a relatively sharp line (at the neutralino mass) above the diffuse galactic background. This is an objective of the recently launched GLAST satellite.

The proton-anti-proton channel presents a challenge since there is an ample background of anti-protons produced by cosmic ray interactions in the interstellar medium. The anti-proton spectrum from Kaluza-Klein particle annihilation, for example, is continuous and shows no special features. It must be observed above the galactic background, and a recent analysis[s6] suggests that for all of the different halo models considered, the dark matter anti-proton signature is well below the galactic background, at energies up to 100 GeV. At higher energies, it may be possible to observe a dark matter signature if the mass of the dark matter particle is low, i.e. ~300 GeV. Balloon (BESS) and space (PAMELA) experiments are currently investigating anti-protons, and these are also one of the goals for the AMS-02 experiment which is awaiting launch.

The e^+-e^- channel is more promising since high energy electrons rapidly lose energy due to synchrotron and inverse Compton processes during propagation in the galaxy. The signature of dark matter here could be either an excess in the total electron (e^+-e^-) spectrum or an increased flux of positrons above the galactic background, or both. Separating electrons from positrons requires a magnetic spectrometer instrument, and one such – HEAT[31] -- reported an excess in the positron to (e^+-e^-) ratio, i.e. the positron fraction, at energies above ~10 GeV. Unfortunately, they did not have the exposure to follow the ratio to higher energy. This observation generated considerable theoretical activity to determine if supersymmetric[s7] or Kaluza-Klein[s8] dark matter annihilation could explain the excess. It was generally agreed that large boost factors (200-300) are required for such explanations. The PAMELA instrument is currently acquiring new positron/electron data.

The final channel is the total electron spectrum, and the present paper is the first to report a significant excess -- a feature -- in the high energy electron spectrum. For a 620 GeV Kaluza-Klein particle annihilation, the feature in the total electron spectrum can be reproduced

with a boost factor of ~200 (depending upon the local density of dark matter[28]) and this same factor could explain the HEAT observations.

Supplementary References:

s1. Chang, J. et al., On the Detection and Identification of Cosmic Gamma-rays in a Cosmic Ray Detector. *26th ICR Conference Papers (Salt Lake City)*, **5**, 37-40, (1999)

s2. Schmidt, W.K.H. et al., On the Identification of High Energy Cosmic Ray Electrons in the Advanced Thin Ionization Calorimeter (ATIC). *26th ICR Conference Papers (Salt Lake City)*, **5**, 41-44, (1999)

s3. Chang, J. et al., High Energy Cosmic Ray Electron Spectra Measured from the ATIC Balloon Experiment, *28th ICR Conference Papers (Hamburg)*, **6**, 2115-2118, (2001)

s4. Nishimura, J. et al., Emulsion chamber observations of primary cosmic-ray electrons in the energy range 30-1000 GeV, *Astrophys. J.*, **238**, 394-409, (1980)

s5. Ganel, O. et al., First Results from ATIC Beam Tests at CERN. *J. Adv. Space Res.*, **27**, 819-824, (2001)

s6. Barrau, A. et al., Kaluza-Klein dark matter and galactic antiprotons, *Phys. Rev. D.*, **72**, 063507, (2005)

s7. Baltz, E.A. and Edsjo, J., Positron propagation and fluxes from neutralino annihilation in the halo. *Phys. Rev. D.*, **59**, 023511, (1998)

s8. Hooper, D. and Kribs, G.D., Kaluza-Klein dark matter and the positron excess. *Phys. Rev. D.*, **70**, 115004, (2004)